

Glutamate Gated Proton-Coupled Electron Transfer Activity of a [NiFe]-Hydrogenase

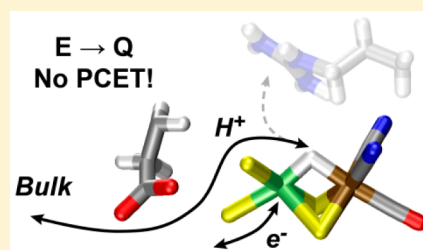
Brandon L. Greene,[†] Gregory E. Vansuch,[†] Chang-Hao Wu,[‡] Michael W. W. Adams,[‡] and R. Brian Dyer^{*†}

[†]Chemistry Department, Emory University, Atlanta, Georgia 30322, United States

[‡]Department of Biochemistry, University of Georgia, Athens, Georgia 30602, United States

S Supporting Information

ABSTRACT: [NiFe] hydrogenases are metalloenzymes that catalyze the reversible oxidation of H₂. While electron transfer to and from the active site is understood to occur through iron–sulfur clusters, the mechanism of proton transfer is still debated. Two mechanisms for proton exchange with the active site have been proposed that involve distinct and conserved ionizable amino acid residues, one a glutamate, and the other an arginine. To examine the potential role of the conserved glutamate on active site acid–base chemistry, we mutated the putative proton donor E₁₇ to Q in the soluble hydrogenase I from *Pyrococcus furiosus* using site directed mutagenesis. FTIR spectroscopy, sensitive to the CO and CN ligands of the active site, reveals catalytically active species generated upon reduction with H₂, including absorption features consistent with the Ni_a-C intermediate. Time-resolved IR spectroscopy, which probes active site dynamics after hydride photolysis from Ni_a-C, indicates the E₁₇Q mutation does not interfere with the hydride photolysis process generating known intermediates Ni_a-I¹ and Ni_a-I². Strikingly, the E₁₇Q mutation disrupts obligatory proton-coupled electron transfer from the Ni_a-I¹ state, thereby preventing formation of Ni_a-S. These results directly establish E₁₇ as a proton donor/acceptor in the Ni_a-S ↔ Ni_a-C equilibrium.



INTRODUCTION

Numerous microorganisms utilize H₂ as an electron source or H⁺ as an electron sink during metabolism through the action of enzymes called hydrogenases (H₂ases).^{1–4} These enzymes are differentiated by their active site metal content as [NiFe], [FeFe], or [Fe]. The active sites of [NiFe] and [FeFe] H₂ases are buried within the protein core, requiring movement of H₂, electrons, and protons through the protein structure.^{5,6} Despite the necessity of long-range proton transfer (PT) and electron transfer (ET) between the active site and protein surface, H₂ases are remarkably efficient and reversible proton reduction catalysts, functioning near the thermodynamic limit with high turnover numbers.^{7–10} A detailed understanding of the structure–function relationship of H₂ases that engenders efficient proton and electron transport, energetic leveling of intermediates, and efficient heterolytic cleavage of H₂ will lead to the development of new catalysts that meet, or exceed, enzymatic function^{11–13} for applications in clean fuel generation.^{14,15}

Mechanistically, [NiFe] H₂ases are best understood because of extensive characterization of their catalytic intermediates and corresponding reactivity (Supporting Information Scheme S1).^{5,6,16,17} It is generally agreed that substrate H₂ is transported through hydrophobic gas channels leading to the active site nickel^{5,6,18–21} and that ET occurs through a chain of closely spaced (<15 Å) redox-active FeS clusters that electronically connect the protein surface and active site.^{5,6,18,22–24} In contrast, while it is clear that the protein

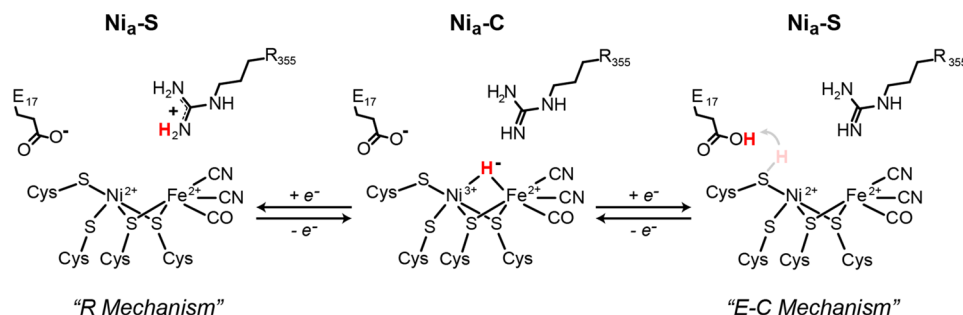
matrix assists PT, neither the residue(s) involved nor their impacts on catalysis are known.^{6,18,25–28} Thus, a significant challenge in understanding the [NiFe] H₂ase catalytic mechanism is the identification of species mediating PT and exploration of their reactivity.

In some postulated PT mechanisms, a cysteine terminally bound to the nickel ion of the active site (Scheme 1) accepts a proton during catalysis as supported by experimental^{28,29} and theoretical studies,^{30–33} and by organometallic model systems.^{34–36} The hypothesis is also circumstantially supported by the natural occurrence of [NiFeSe] H₂ases, which contain a terminal selenocysteine in place of a cysteine and exhibit higher overall activity, lower product inhibition, and enhanced O₂ tolerance.^{37–40} Multiple PT pathways connecting a protonated cysteine thiol to the protein surface have been hypothesized based on X-ray crystallography,^{5,18,28,41–43} site directed mutagenesis in conjunction with spectroscopic and kinetic methods,^{44,45} and theoretical simulations.^{26,27,46} Such studies support a pathway immediately beyond the first coordination sphere of the nickel ion involving a conserved glutamate adjacent to a terminal cysteine (E–C mechanism in Scheme 1).

Another hypothesis is that a conserved arginine, located above the [NiFe] bridging substrate position, may also function in proton transport (R mechanism in Scheme 1). This residue has recently been proposed to function together with the active

Received: July 27, 2016

Published: September 12, 2016

Scheme 1. Proposed PT Pathways at the [NiFe] Hydrogenase Active Site^a

^aMigrating proton is depicted in red, and transient cysteine protonation is shaded.

site as a frustrated Lewis pair to polarize and heterolytically cleave H₂;⁴⁷ thus, it is reasonable to hypothesize it may become protonated after H–H bond cleavage. Once protonated, this arginine must then exchange protons with bulk solvent to maintain catalysis. A hydrogen bonded network has been examined which may facilitate proton exchange from arginine to the protein surface.⁴⁸ This mechanism is particularly appealing because it is analogous to PT at the active site in [FeFe] H₂ases^{6,49–51} and is similar to biomimetic synthetic catalysts containing pendant amines for proton reduction.^{11,12,52} Arginine is an uncommon base in enzyme catalysis with a very high pK_a that is not significantly tuned by the surrounding environment because of the delocalization of the positive charge.⁵³ Nevertheless, there are examples of enzymes in which arginine functions in this way.⁵⁴

It is unclear which of the two potential PT mechanisms (Scheme 1) is responsible for efficient PT and H₂ activation in [NiFe] H₂ases. The thermodynamic implications of the two mechanisms are significant because the pK_a of glutamate and arginine differ by >8 units in solution. Additionally, PT at the active site is coupled to ET during turnover (proton-coupled electron transfer, PCET),^{17,55} and thus the substantial difference of the two pathways has significant impact on the (PC)ET thermodynamics and kinetics.

We have previously examined the PCET chemistry at the active site of soluble hydrogenase I (SHI) from *Pyrococcus furiosus* (Pf) through photoreduction and hydride photolysis dynamics.^{17,55} These studies demonstrated that concerted PCET occurs during the transition between catalytic intermediates Ni_a-S and Ni_a-I, which rapidly forms Ni_a-C (Supporting Information Scheme S1), and that this transition is modulated by an amino acid residue adjacent to the active site with pK_a ≈ 7. We hypothesized this amino acid is the conserved glutamate (E₁₇, Pf SHI numbering). Herein, we directly confirm this hypothesis by site directed mutagenesis (SDM), mutating E₁₇ to the structurally similar, but nonionizable amino acid glutamine (E₁₇Q). Using steady state and time-resolved spectroscopy, we demonstrate that although the E₁₇Q SHI active site displays a distribution of putative catalytically active states, it cannot facilitate the PCET required for the Ni_a-S ↔ Ni_a-C transition, identifying E₁₇ as the proton acceptor adjacent to the terminal cysteine in the [NiFe] H₂ase active site.

EXPERIMENTAL METHODS

Materials. Potassium phosphate monobasic, potassium phosphate dibasic, MES, EPPS, myoglobin, and sodium dithionite were purchased from Sigma-Aldrich. H₂(5%)/N₂(95%) and N₂(99.9999%) were purchased from Nexair. Amicon centrifugal protein concentrators were purchased from EMD Millipore.

Construction, Expression, and Purification of E₁₇Q. The plasmid encoding the E₁₇Q variant of PF0894 (encoding SHI) was constructed by following the protocol of the QuikChange II Site-Directed Mutagenesis Kit (Agilent Technologies). The site mutated gene was amplified from the sequence confirmed plasmid and assembled with the *pyrF* selection marker, P_{slp} as the promoter, a 9x-His tag at the N-terminus, and upstream (UFR) and downstream flanking (DFR) region by overlapping PCR as previously reported.⁵⁶ The flanking regions were targeted at the PF0574-PF0575 intergenic space. By homologous recombination, the linear knock-in cassette was transformed into MW0015 ($\Delta pyrF \Delta shIbgda \Delta shIIIbgda$) as shown in Supporting Information Figure S1. MW0015 does not contain any cytoplasmic hydrogenase activity, so the activity of the E₁₇Q SHI could be quickly screened by measuring hydrogen evolution activity in the cytoplasmic extract (S100). The sequence-confirmed clone (MW0505) was used for large-scale fermentation, protein purification, and characterization as previously reported.⁵⁶ Briefly, cells harvested from a 20-L fermentation were lysed in 50 mM Tris buffer, pH 8.0, containing 2 mM dithiothreitol (DTT) and 50 μg/mL DNase with a cell (g, wet weight) to buffer (ml) ratio of 1:5 in an anaerobic chamber. The S100 obtained after ultracentrifugation was directly loaded on a Ni-NTA column and the bound protein was obtained by gradient elution. The hydrogenase was further purified by QFF chromatography and used for spectroscopic characterizations.

SHI H⁺ Reduction Activity Measurements. The proton reduction activity of E₁₇Q SHI was measured as previously reported with only minor modification.¹⁷ Assays were carried out in anaerobic glass vials with 2 mL of 100 mM EPPS buffer, pH 8.4. 1 mM methyl viologen reduced by 10 mM DT was used as the electron donor, and the assays were performed at 80 °C for 6 min. Hydrogen production was analyzed by a 6850 Network Gas Chromatography (GC) system from Agilent technologies. One unit (U) of activity is equal to 1 μmol of H₂ produced min⁻¹.

SHI H₂ Oxidation Activity Measurements. The enzyme was activated by incubation under hydrogen for 2 h. A stirred solution of 71–142 nM hydrogenase at 25 °C, pH 7.5 50 mM phosphate buffer was saturated with hydrogen gas in a low volume cuvette. Injection of 3.4 mM methyl viologen initiates hydrogen oxidation, which is monitored by growth of the reduced methyl viologen absorbance at 605 nm ($\epsilon \approx 14500 \text{ cm}^{-1} \text{ M}^{-1}$). Independently, a similar procedure was followed to monitor benzyl viologen reduction at 80 °C in a sealed assay vial containing pH 8.4 100 mM EPPS and 1 mM benzyl viologen. The growth of reduced benzyl viologen was monitored at 580 nm ($\epsilon \approx 8800 \text{ cm}^{-1} \text{ M}^{-1}$). All measurements were repeated in triplicate. Turnover frequencies and specific activity indicate E₁₇Q activity is ~19% that of WT.

Sample Preparation for Spectroscopy. Sample preparation for the E₁₇Q SHI for UV–vis, FTIR, and transient infrared (TRIR) spectroscopy were performed in an anaerobic glovebox containing 4% H₂ in N₂ identically as previously reported for WT SHI.^{17,55} Briefly, 3 mg of E₁₇Q SHI were buffer exchanged into the desired buffer (10 mM MES for pH 6.5, 100 mM KP_i for pH 7.5, and 100 mM EPPS for pH 8.5) pre-equilibrated with the glovebox atmosphere by 5-fold concentration–dilution cycles using an Amicon 50 kDa molecular

weight cutoff centrifuge filter. After being buffer exchanged, samples were concentrated to a final volume of 15–20 μL ($\sim 1\text{--}2\text{ mM}$) and loaded into a 75 μm path length IR transmission cell.⁵⁵ The reference was prepared by dissolving 4.8 mg of horse heart myoglobin into the desired buffer, reducing it with dithionite and concentrating it in an Amicon 3 kDa filter to 50 μL ($\sim 5\text{ mM}$) in order to match the optical density of the sample at 532 nm. After loading the sample and reference, the transmission cell was sealed anaerobically. This sample preparation protocol was used for all measurements.

UV–vis Spectroscopy. UV–vis spectra were measured on a home-built single beam transmission based fiber coupled system with an Ocean Optics QE65000 thermoelectric cooled CCD spectrometer and a 30 W xenon lamp,^{17,55} or on a PerkinElmer Lambda 35 UV/vis spectrometer.

FTIR Spectroscopy. FTIR spectra were measured at room temperature on a Varian 660 FTIR spectrometer (Agilent Technologies, Inc.), at 2 cm^{-1} resolution and baseline subtracted.^{17,55}

FTIR spectra were fit in the ν_{CO} region by four to five pseudo-Voigt functions.⁵⁵

TRIR Spectroscopy. TRIR measurements were performed on the same samples used for the UV–vis and FTIR measurements. They were performed as previously described, with minor modifications.⁵⁵ Briefly, the nanosecond TRIR system employs the second harmonic (532 nm) of a Surelight Nd:YAG (Continuum, Inc.) as the excitation source and a tunable quantum cascade laser (Daylight Solutions, Inc.) as the probe source. The infrared detector is a 1 mm mercury cadmium telluride element with a 20 MHz preamplifier and a 100 ns rise time (Kolmar Technologies, Inc.). The sample excitation energy was set between 200 and 450 $\mu\text{J}/\text{pulse}$ and focused to a 350 μm –1 mm diameter spot giving an energy density of 50–400 mJ/cm^2 . The QCL probe was focused to a 90 μm diameter spot and overlapped with the pump by maximizing the solvent heating signature induced by the nonradiative decay of pump pulse absorption in either the myoglobin reference or the H_2ase sample solution.

The solvent heating background signal is removed from the sample transient by subtracting the reference transient containing the identical background solvent heating signature.¹⁷ Before subtraction, the reference heating signature was normalized to the sample between 200 and 800 μs , which is well separated from the H_2ase transient dynamics. Optical feedback creates noise in the QCL output that is observed between 200 μs and 10 ms. This noise gives rise to $\sim 20\ \mu\text{OD}$ oscillations around zero absorbance. To avoid lifetime measurement error associated with incorrect baseline weighting, single wavelength transients were fit to single exponentials from 100 ns to 100 μs , which for the photochemical process measured in this work is at least 20 lifetimes, giving ample data for accurate lifetime fitting. Single wavelength absorption transients were temporally binned between 100–500 ns and 5–10 μs at each wavelength to generate a transient spectrum. The transient spectrum was fit by three pseudo Voigt functions analogous to the fitting procedure used for FTIR fitting.

Temperature dependent transient measurements were obtained by modulating the temperature of the sample with an externally controlled recirculating water bath (Thermo Fisher Scientific, Inc.). Target temperatures were set on the water bath, and the temperature at the sample during data acquisition was determined by a thermocouple directly attached to the IR transmission cell.

RESULTS

The E_{17}Q *Pf* SHI was prepared by site directed mutagenesis, purified to homogeneity by affinity chromatography and assayed for H^+ reduction activity by the dithionite-methyl viologen assay as described in the Experimental Methods. The H_2 evolution activity of the E_{17}Q exchanged enzyme was ca. 10% compared to wild type (WT, Supporting Information Figure S2). Similar residual activity has been previously reported for mutations of the distal glutamate in $[\text{NiFe}]\text{-H}_2\text{ases}$.⁴⁵ The basal H^+ reduction activity of the E_{17}Q exchanged enzyme indicates that despite significant attenuation,

the E_{17}Q SHI is still capable of reducing protons and thus the capacity to transfer protons to and from the active site can still occur, albeit at diminished levels. The H_2 oxidation activity of the E_{17}Q SHI was 19% compared to WT (Supporting Information Figure S3), shifting the catalytic bias toward H_2 oxidation as observed when using soluble redox mediators. The difference in attenuation of H_2 oxidation versus H_2 production rates can be rationalized by observations that the two reactions have different rate-determining steps.⁵⁷ A similar, but more dramatic attenuation of H_2 oxidation activity has been reported for the conserved arginine residue; thus, PT and catalysis may not follow one single pathway exclusively.⁴⁷ The observation of attenuation of activity in both enzyme variants highlights the shortcomings of a purely activity based assessment of the mutational effect.

To further probe the mechanistic implications of the E_{17}Q exchange, we examined the FTIR spectrum of the $[\text{NiFe}]$ active site in the ν_{CO} region. The FTIR spectra of WT and E_{17}Q *Pf* SHI prepared identically at pH 7.5 in an atmosphere of 4% H_2 in N_2 are compared in Figure 1. The WT spectrum (Figure 1

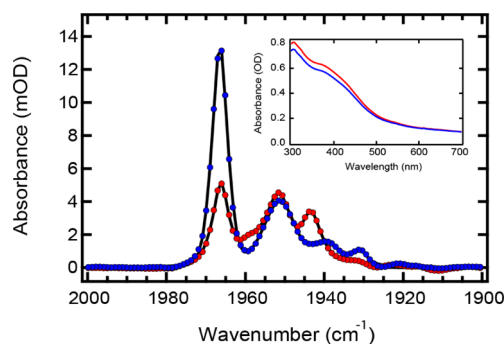


Figure 1. FTIR and UV–vis spectrum of the WT (blue) and E_{17}Q (red) *Pf* SHI in 4% H_2 atmosphere at pH 7.5 and associated fits to experimental data (black lines). The data were fit to a function containing five independent pseudo-Voigt components. Inset shows UV–vis spectra of WT (blue) and E_{17}Q (red) *Pf* SHI prior to FTIR characterization.

blue circles, reproduced from ref 55) reveals a mixture of chemically and kinetically competent active states, the most clearly resolved corresponding to $\text{Ni}_a\text{-C}$ (1966.8 cm^{-1}) and $\text{Ni}_a\text{-SR}$ (1952.7 cm^{-1}) as well as minor peaks consistent with $\text{Ni}_a\text{-S}$ (1946.8 cm^{-1}) and the ready but inactive $\text{Ni}_i\text{-S}$ (1931.3 cm^{-1}) and $\text{Ni-SR}'$ (1939.3 cm^{-1}) states (summarized in Supporting Information Table S1).^{17,55,58,59} By comparison, the FTIR spectrum of the E_{17}Q enzyme (Figure 1 red circles) displays significantly less overall ν_{CO} amplitude and a distinct equilibrium peak distribution. The decreased total ν_{CO} amplitude cannot be accounted for by a difference in enzyme concentration, as the UV–vis spectra of the WT and E_{17}Q samples are nearly identical in the FeS cluster absorption region ($\lambda < 600\text{ nm}$, Figure 1 inset). This observation may indicate a role for E_{17} in $[\text{NiFe}]$ active site assembly and incorporation. The FTIR spectrum of E_{17}Q contains bands that correspond to $\text{Ni}_a\text{-C}$ (1966.2 cm^{-1}), $\text{Ni}_a\text{-SR}$ (1951.4 cm^{-1}), $\text{Ni-SR}'$ (1943.2 cm^{-1}), and $\text{Ni}_i\text{-S}$ (1932.8 cm^{-1}), all of which are shifted slightly from WT enzyme. The $\text{Ni-SR}'$ species is the most shifted relative to WT ($\sim 4\text{ cm}^{-1}$) and may indicate some population of $\text{Ni}_i\text{-S}$ which is not clearly resolved by spectral fitting. The presence or absence of $\text{Ni}_a\text{-S}$ is not apparent from the FTIR fitting, although due to the low concentration of $\text{Ni}_a\text{-S}$ in WT

samples as well as the lower signal-to-noise and spectral congestion of the $E_{17}Q$ spectrum, its presence cannot be ruled out. A small amplitude resonance at $\sim 1958\text{ cm}^{-1}$ is also observed, which is most closely associated with the oxygen inhibited Ni_a -B state.^{58,60} Comparison of the two FTIR spectra over the entire ν_{CO} and ν_{CN} absorption envelope as well as second derivative spectra are reported in the Supporting Information Figures S4 and S5, respectively.

The ν_{CO} resonances of the Ni_a -S and Ni_a -C states in the WT enzyme are shifted by changing the pH between pH 6–8.⁵⁵ This effect is attributed to two distinct phenomena occurring over a very narrow pH range. The first contribution to the shift is derived from the pH dependent redox potentials of both the Ni_a -S \leftrightarrow Ni_a -C and Ni_a -C \leftrightarrow Ni_a -SR transitions, which are proton coupled transitions that shift with pH in a nearly Nernstian fashion.^{61–63} In contrast, the reduction potentials of FeS clusters are nearly pH independent.⁶⁴ As a consequence, when modulating pH at fixed reductant concentration (H_2), the redox equilibrium between the proximal FeS cluster and [NiFe] active site shifts toward FeS reduction at high pH. Reduction of the proximal FeS cluster results in a slight increase in electron density at the [NiFe] active site, a concomitant increase in π^* back-bonding in the Fe–C(O) bond, and a red shift of the ν_{CO} band. The second phenomenon is an acid–base equilibrium near the active site.⁵⁵ This equilibrium modulates a hydrogen bond to the active site, presumably to one of the active site thiolates. Elimination of this hydrogen bond at high pH increases the electron density at the active site, resulting in a red shift of the ν_{CO} band analogously as above. The two processes are observed over a very narrow pH or potential window, making them difficult to deconvolve by steady state techniques. The pH dependent Ni_a -C state resonance of the $E_{17}Q$ SHI shifts -0.8 cm^{-1} between pH 6.5 and 8.5 (Supporting Information Figure S6) whereas the WT enzyme is shifted -1.5 cm^{-1} over a similar range.⁵⁵ Apparently, the $E_{17}Q$ substitution turns off the acid–base equilibrium such that only the pH dependent redox potentials contribute to the shift in this case.

The Ni_a -C state is inherently photosensitive, and under illumination the metal bridging hydride can be photolyzed by reductive elimination to produce a proton and a formal Ni^{1+} species at the [NiFe] active site termed Ni_a -I^(1/2) (previously termed Ni-L).^{17,55,65,66} This Ni_a -I species represents an obligatory intermediate in the conversion of Ni_a -S \leftrightarrow Ni_a -C^{17,55,67} and can be stabilized in the absence of light in certain enzymes and experimental conditions.^{68–70} Thus, the redefinition of “Ni-L” to “ Ni_a -I” addresses these recent findings and follows established [NiFe] H_2 ase intermediate nomenclature, where the subscript “a” indicates this species is an active state in catalysis, and the “I” indicates a paramagnetic fleeting intermediate rather than a metastable paramagnetic intermediate (like Ni_a -A/ Ni_a -B/ Ni_a -C) or light induced artifact (Ni-L). In the WT *Pf* SHI, at pH > 6.5 and in conditions where the proximal FeS cluster remains oxidized, the Ni_a -I¹ state can form Ni_a -S with a rate constant of $1.8 \times 10^5\text{ s}^{-1}$ at 20 °C via a PCET mechanism (Supporting Information Scheme S1, Figure 2). The transiently formed Ni_a -S state then relaxes back to Ni_a -C on the 100 μ s time scale.⁵⁵ Our hypothesis that E_{17} functions as the base during the aforementioned PCET reaction would thus be most clearly tested by examining the photochemistry of $E_{17}Q$. Figure 2 shows the transient spectrum of $E_{17}Q$ prior to Ni_a -S formation in WT (100–500 ns) and at the peak of Ni_a -S formation in WT (5–10 μ s) after 532 nm excitation. Between

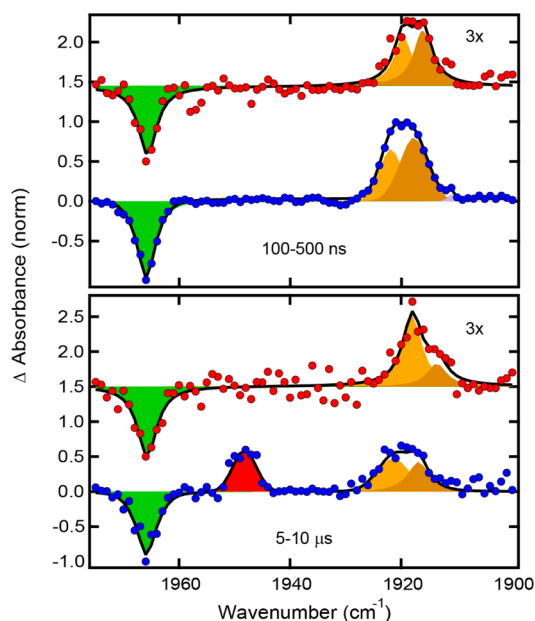


Figure 2. Normalized transient IR spectrum of $E_{17}Q$ (red circles) and WT (blue circles) *Pf* SHI at pH 7.5 between 100 and 500 ns (top) and 5–10 μ s (bottom) after 532 nm excitation and associated fit to the experimental data (black lines). Fit components are represented as shaded Voigt profiles for Ni_a -C (green), Ni_a -S (red), Ni_a -I¹ (orange), and Ni_a -I² (tan). The $E_{17}Q$ data are scaled by a factor of 3 for comparison to WT data and offset from the baseline for clarity.

100 and 500 ns we observe a single bleach feature at 1965.7 cm^{-1} , indicating Ni_a -C is photolyzed in the $E_{17}Q$ enzyme. In addition, two induced absorbance features were observed at 1916.2 and 1919.7 cm^{-1} with approximately equal amplitude, very similar to the Ni_a -I¹ (1918 cm^{-1}) and Ni_a -I² (1922 cm^{-1}) states of the WT enzyme at pH 7.5. Interestingly, we also observed a small transient absorption at 1913 cm^{-1} that is potentially associated with a small bleach at 1959 cm^{-1} , which may represent an alternative Ni_a -C like state in the $E_{17}Q$ SHI.

The spectrum generated at a later time (5–10 μ s, Figure 2), where significant Ni_a -S formation is observed in the WT SHI at this pH (Supporting Information Figure S7), exhibits no evidence for Ni_a -S formation despite the $E_{17}Q$ enzyme being more oxidized than the WT enzyme (Figure 1 inset). The transient spectrum of the Ni_a -I¹ and Ni_a -I² species between 5 and 10 μ s shows a slight shift relative to the 100–500 ns spectrum, which is not manifested in the Ni_a -C state bleach. This could be due to a change in the local environment of these species on this time scale. An alternative explanation, that the spectral shift is an artifact caused by the low signal-to-noise ratio and biasing of the curve fitting by the persistent small induced absorption feature at 1913 cm^{-1} (*vide supra*), is also possible. Based on our previous experiments with WT *Pf* SHI, we favor the latter explanation. At pH 6.5 and 8.5 under similar conditions the $E_{17}Q$ SHI forms both Ni_a -I¹– Ni_a -I² instantaneously after excitation at approximately equal populations (Supporting Information Figure S8) and no Ni_a -S formation is observed at any time during hydride recovery (Supporting Information Figure S9).

The kinetic evolution of the Ni_a -I¹ and Ni_a -I² states at pH 7.5 was further examined by single wavelength kinetics at 1916 and 1920 cm^{-1} respectively. Ni_a -C was also examined (1966 cm^{-1}) to establish a kinetic understanding of the photochemical reaction (Figure 3). In the WT enzyme, decay kinetics for Ni_a -

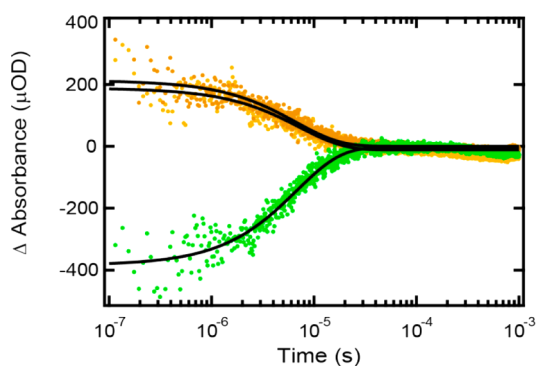


Figure 3. Single wavelength transients of E₁₇Q SHI monitored at 1915 cm⁻¹ (tan dots), 1921 cm⁻¹ (orange dots), and 1966 cm⁻¹ (green dots) after 532 nm laser excitation and associated monoexponential fits to experimental data (black lines). Small baseline fluctuations beyond 200 μs are due to laser feedback noise.

I¹ and Ni_a-I² are observed to be monoexponential, whereas the Ni_a-S (transient formation and decay) and Ni_a-C (recovery) dynamics are observed to be biexponential.^{17,55} For the E₁₇Q SHI, decay of both Ni_a-I¹ and Ni_a-I² as well as recovery of Ni_a-C were modeled well by single exponentials with nearly identical rate constants within error ((1.39–1.51) × 10⁵ s⁻¹), indicating no additional intermediates are populated in the reformation of Ni_a-C from the Ni_a-I states and rapid interconversion between Ni_a-I¹ and Ni_a-I² is maintained in the E₁₇Q SHI (Figure 3). In summary, there is no evidence of Ni_a-S formation over the time course of the measurements based on transient spectra at pH 6.5, 7.5, and 8.5, by single wavelength analysis of Ni_a-S probed at 1950 cm⁻¹ (Supporting Information Figure S10) and by kinetic analysis of Ni_a-C reformation. PCET to form Ni_a-S requires that a nearby FeS cluster be oxidized, which can accept the outgoing electron in the Ni_a-C → Ni_a-S transition. Based on the nearly identical UV–vis features of the WT and E₁₇Q samples at pH 7.5 (Figure 1 inset), we conclude that they should have equal probability of ET and thus the E₁₇ to Q mutation does not impede the ET step of the PCET, but rather the PT step.

Finally, we have investigated the thermodynamics of the resultant Ni_a-C ↔ Ni_a-I tautomerization in the E₁₇Q SHI by temperature dependent kinetic analysis of hydride recovery at pH 6.5 and 8.5 (Supporting Information Figure S11). In the WT enzyme, the barrier measured at basic pH, where the ancillary [FeS] clusters are reduced and thus PCET mediated oxidation of Ni_a-I¹ cannot occur, was determined to be 32 kJ/mol. The barrier at high pH is significantly smaller than that measured at pH < 7 (40 kJ/mol). At low pH, the PCET equilibrium between Ni_a-I¹ and Ni_a-S raises the apparent barrier for hydride recovery, since this coupled process also contains a small, but appreciable barrier (E_a = 6.1 kJ/mol).⁵⁵ Thus, the difference in apparent barrier at low and high pH reports on the additional PCET competent pathway in the WT SHI. The apparent barrier for hydride reformation of the E₁₇Q SHI at both pH 6.5 and 8.5 were measured to 36 ± 2 and 38 ± 2 kJ/mol respectively (Supporting Information Figure S11). The two barriers, one above and the other below the redox couple of the proximal FeS cluster, are slightly larger than that observed for the WT enzyme. The lack of difference in apparent barrier for the two pH extremes indicates the hydride recovery mechanism is identical at low and high pH, with no additional coupled chemical pathways (only Ni_a-I¹ ↔ Ni_a-C).

The larger barrier for hydride recovery in the E₁₇Q SHI (average of 37 kJ/mol) relative to WT (32 kJ/mol) may be due to stabilization of the Ni_a-I states by a different H-bonding character of the E₁₇Q mutation, which can donate or accept H-bonds, potentially stabilizing the Ni_a-I^(1/2) state(s).

DISCUSSION

The aggregate evidence of site directed mutagenesis, steady state as well as transient spectroscopy, kinetics, and thermodynamics of hydride photolysis and recovery is consistent with the previously proposed E-C mechanism for PT in the Ni_a-S ↔ Ni_a-C transition, as illustrated in Scheme 1.⁵⁵ In this mechanism, PCET from Ni_a-C to form Ni_a-S occurs in two distinct steps. Initially, the Ni_a-C state tautomerizes to form an isoelectronic Ni_a-I^(1/2) state via reductive elimination, and thus the charge on the extended active site remains constant. This transition is proposed to be a Ni³⁺-H⁻ (Ni_a-C) to Ni²⁺ + H⁻ (Ni_a-I^(1/2)) transition,⁶ but the location of the proton has been, until now, unclear. Despite having significant ramifications on rapid and reversible interconversion of Ni_a-S and Ni_a-C, the E → Q substitution does not completely abolish H₂ oxidation or H₂ production activity indicating that protons can still exchange with the active site.

For “standard” (O₂-sensitive or O₂-intolerant) [NiFe] H₂ases, Ni_a-C is dominant over the Ni_a-I state in solution at potentials where both could exist. In contrast, in the O₂ tolerant [NiFe] H₂ases the transition between Ni_a-C and Ni_a-I is achievable under a variety of conditions, and enhanced significantly above pH 7.^{71–73} One explanation for this difference could be the subtle weakening of the Ni³⁺-H⁻ bond strength in the O₂-tolerant [NiFe] H₂ases,⁷³ decreasing its pK_a. Thus, the barrier for the tautomer interconversion is expected to be reasonably low, even in the standard [NiFe] H₂ases, a critical requirement for rapid and reversible catalysis. Despite the more tightly bound hydride in the “standard” H₂ases, they exhibit higher activity in both H⁺ reduction and H₂ oxidation. This observation seems counterintuitive, but the rate of tautomerization is very rapid relative to turnover, and therefore there may be alternative explanations for the enhanced activity of “standard” [NiFe] H₂ases.

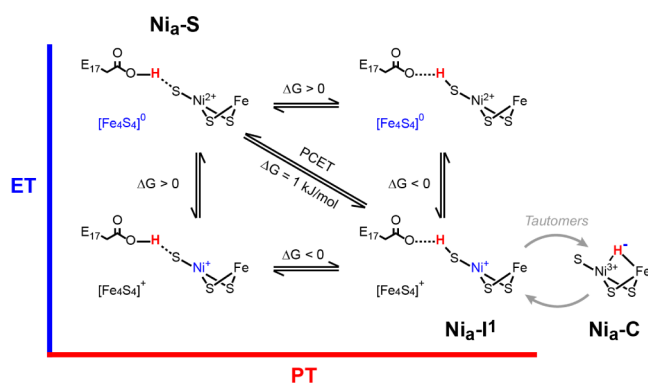
The closest base to the hydride ligand is the terminally coordinated cysteine thiolate at ca. 2.5 Å.³ The next closest base is the bridgehead arginine, with the δN atom being 3.6 Å away.⁵ Experimental evidence indicates the base that accepts the proton in the Ni_a-C ↔ Ni_a-I transition is the nickel thiolate,^{29,74} but this conclusion was based largely on DFT modeling of spectral properties of the Ni_a-I state. Thiolate as the proton acceptor makes sense chemically based on its closer proximity relative to the arginine and the higher pK_a expected for the Ni⁺ coordinated thiolate compared to Ni²⁺ or Ni³⁺.

A critical distinction between the two possible proton acceptors in the tautomerization of Ni_a-C to Ni_a-I is immediately clear when considering the second step necessary in Ni_a-C ↔ Ni_a-S conversion, (PC)ET. If the hydride dissociates to the bridgehead arginine upon tautomerization, direct ET from Ni⁺ to the proximal FeS cluster would result in Ni_a-S formation (R mechanism). This process would thus be pH independent and have no kinetic isotope effect (KIE). Alternatively, in the E-C mechanism (Scheme 1) the conversion of Ni_a-I to Ni_a-S would involve a PCET event, as the terminal cysteine is believed to be deprotonated in the Ni_a-S state,^{6,32} although some theoretical studies favor a permanently protonated thiol at the terminal position trans

to the hydride.^{30,33} In the E–C mechanism, the terminal thiol would not be solvent exchangeable due to the requirement for subsequent PCET, fully consistent with experimental observations from spectroelectrochemistry.⁷¹ We have previously observed a KIE of >40 for the $\text{Ni}_a\text{-I}^1 \leftrightarrow \text{Ni}_a\text{-S}$ interconversion, indicative of a concerted PCET event with significant nuclear tunneling, whereas the KIE for $\text{Ni}_a\text{-I}^{(1/2)} \rightarrow \text{Ni}_a\text{-C}$ is only 3.^{17,55} In addition, the KIE of the $\text{Ni}_a\text{-I} \leftrightarrow \text{Ni}_a\text{-S}$ transition is pH dependent and correlated with the pH dependent shift of the $\text{Ni}_a\text{-C}$ ν_{CO} resonance, which was postulated to be associated with acid–base chemistry of an adjacent hydrogen bonded residue (E_{17}).^{17,55} The data presented herein demonstrate that, upon substitution of Q for E_{17} , all PCET chemistry is shut down, validating the E–C mechanism and the central role of an E–C dyad in facilitating concerted PCET at the active site remote from the nickel.

Within this model, it is possible to address the PCET chemistry of the $[\text{NiFe}]$ H_2 ases from a thermochemical perspective. Scheme 2 describes a “square scheme” for potential

Scheme 2. Square Scheme for PCET between $\text{Ni}_a\text{-S}$ and $\text{Ni}_a\text{-I}^1$ ^a

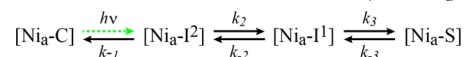


^aActive proton involved in PT is shown in red, and electron involved in ET shown in blue. $\text{Ni}_a\text{-I}^1$ and $\text{Ni}_a\text{-I}^2$ are isoelectronic tautomers. ΔG is expressed for each reaction as written from left to right or top to bottom.

PCET pathways within the E–C mechanism. PCET can occur via a ET–PT (down then right), PT–ET (right then down), or concerted PCET (diagonal) mechanism.^{75–77} As detailed above, the experimental evidence strongly supports the concerted reaction.^{17,55} Considering our previous measurements of the pK_a of E_{17} at ~ 7 in the WT *Pf* SHI as well as the known reduction potential of the redox active FeS cluster,^{55,78,79} it becomes clear why the concerted pathway is thermodynamically advantageous. Since the PT active terminal cysteine appears to remain thiolate in character in the $\text{Ni}_a\text{-S}$ state, the pK_a is anticipated to be lower than 7; thus, PT from E_{17} would be unfavorable ($\Delta G^0 > 0$) making a PT–ET mechanism unfavorable. In addition, reduction of $\text{Ni}_a\text{-S}$ is likely unfavorable since no Ni^+ states are observed without a coupled PT event, consistent with reduction potentials of biomimetic model compounds in the absence of an acid.^{80–83} Thus, the coupling of ET to PT in a concerted step allows for low barrier interconversion of $\text{Ni}_a\text{-S}$ and $\text{Ni}_a\text{-I}$. With the flurry of recent advances in synthetic modeling of the $[\text{NiFe}]$ active site,^{81–86} it will be interesting to compare pK_a values of hydrides and terminal thiols with reduction potentials of model compounds

and their capacity for concerted PCET chemistry relevant to that observed in H_2 ase.

In the WT enzyme, the photochemical reaction following laser excitation of $\text{Ni}_a\text{-C}$ can be described by the equilibria:⁵⁵



After excitation, formation of $\text{Ni}_a\text{-I}^1$ from $\text{Ni}_a\text{-I}^2$ is spontaneous and competitive with $\text{Ni}_a\text{-I}^2$ decay back to $\text{Ni}_a\text{-C}$. This necessitates that ΔG_{PCET} from $\text{Ni}_a\text{-I}^1$ to $\text{Ni}_a\text{-S}$ be negative. During the photochemical evolution between 10 and 20 μs the population of $\text{Ni}_a\text{-S}$ remains essentially unchanged (because $k_{-1} \approx k_3$, $k_3 > k_{-3}$, and $\text{Ni}_a\text{-I}^{1/2}$ rapidly interconvert);^{17,55} thus, the final step in this scheme establishes a pre-equilibrium ($d[\text{S}]/dt = 0$) before the system returns to the initial state. Under this condition, the value of ΔG_{PCET} can be calculated from eqs 1 and 2,

$$K_{\text{eq}}(3) = \frac{k_3}{k_{-3}} = \frac{[\text{Ni}_a\text{-S}]}{[\text{Ni}_a\text{-I}^1]} \quad (1)$$

$$\Delta G_{\text{PCET}} = -R \cdot T \cdot \ln[K_{\text{eq}}(3)] \quad (2)$$

where R is the gas constant and T is the temperature in Kelvin. Using the transient spectrum generated at the 10–20 μs time scale and quantifying the relative concentrations of $\text{Ni}_a\text{-S}$ and $\text{Ni}_a\text{-I}^1$ based on their integrated intensities (scaled for wavelength dependent M–CO oscillator strength)⁸⁷ we can solve these equations, yielding a ΔG_{PCET} of -1 kJ/mol, which is consistent with the minimal energetic differences between these states from theory.^{31,32} We have also measured a small activation barrier of 6 kJ/mol for the reverse reaction.¹⁷ Thus, the concerted PCET reaction creates a nearly barrierless (5 kJ/mol) transition between two energetically very similar states, $\text{Ni}_a\text{-S}$ and $\text{Ni}_a\text{-I}^1$, a hallmark of efficient and reversible catalysis.

Based on the initial population of $\text{Ni}_a\text{-I}^1$ and $\text{Ni}_a\text{-I}^2$ and their coupled decay kinetics, these two states are nearly isoenergetic and rapidly interconvert. We have previously interpreted the interconversion to be due to a H-bond isomerization, where, in the $\text{Ni}_a\text{-I}^1$ form, the thiol forms a H-bond with the PT partner (now established to be E_{17}), a prerequisite for H^+ tunneling. In the $\text{Ni}_a\text{-I}^2$ state this bond is broken and the glutamate of E_{17} instead may form H-bonds to the hydroxyl group of a threonine and the backbone NH of an alanine. The latter H-bonding configuration is observed in most X-ray structures of the $[\text{NiFe}]$ H_2 ases,⁵ which displays some disorder in certain structures implying multiple conformations.⁴³ Further data from site directed mutagenesis targeting this threonine has shown that it facilitates $\text{Ni}_a\text{-S}$ formation, modulates the glutamate conformation, and is important in proper enzyme function and H^+ exchange.⁸⁸ Rapid H-bond isomerization between $\text{Ni}_a\text{-I}^1$ and $\text{Ni}_a\text{-I}^2$ is plausible since the H-bonding character of thiols and thiolates are relatively weak. Since the $\text{Ni}_a\text{-I}^1 \leftrightarrow \text{Ni}_a\text{-I}^2$ equilibrium reaches steady state faster than the 100 ns time resolution of the methods reported herein, ultrafast infrared spectroscopy will be required to unravel the dynamics of the initial events in hydride photolysis. The subsequent oxidative addition of the thiol proton to Ni^+ forming the $\text{Ni}_a\text{-C}$ state is downhill, as is clear from the steady state populations of $\text{Ni}_a\text{-C}$ and $\text{Ni}_a\text{-I}^{(1/2)}$, but there is a barrier of 32 kJ/mol for this reaction. Importantly, the conservative $\text{E}_{17}\text{-Q}$ substitution is expected to maintain some degree of H-bonding character, while also potentially donating H-bonds through the amide

NH₂ group. Thus, E₁₇Q is expected to have a similar photoproduct distribution, but no PCET chemistry, consistent with our observations.

It is critical to the present analysis that the E → Q mutation minimally perturbs the active site environment and solely inhibits proton transfer by the dramatic increase in pK_a of the Q side chain relative to E. Two potential alternative perturbations could occur which may affect the PCET chemistry observed during hydride photolysis: (1) the structure could be perturbed such that the native proton acceptor is structurally incapable of accepting the proton or (2) the mutation may modulate the active site reduction potential affecting the ET component of the PCET event. The structural perturbations of active site resulting from the E₁₇Q exchange appear to be small from the infrared spectrum of the mutant, which displays numerous known intermediates that appear very similar to the WT enzyme. The hydride photolysis dynamics, including recombination kinetics and thermodynamics, are also preserved in E₁₇Q. The E → Q exchange has been structurally characterized in the [NiFe] H₂ase from *D. fructosovorans*,⁴⁵ as well as numerous other residues along the proposed PT pathway terminating with the conserved glutamate.⁸⁸ The structural perturbation induced by the Q substitution is minimal, with an approximately 0.3 Å elongation of the O–S distance between Q and C side chains. To our knowledge all of the structures reported to date for [NiFe] H₂ases contain O–S distances too long to be formal H-bonds. It must then be inferred that structural rearrangements would be required for efficient PCET. This is consistent with the high temperature factors observed for both glutamate and cysteine side chains observed in the native crystal structures of [NiFe] H₂ases.⁵ Our previous work^{17,55} suggests this conformation must be dynamic in order to facilitate the observed PCET via proton nuclear tunneling. As such, the resting structure observed by crystallography probably does not represent the PCET active conformation.

As noted previously, it must also be considered that the E → Q substitution may affect the electronic properties of the active site, which in turn affect the active site oxidation potential and therefore modulate the (PC)ET rate. The necessary electronic perturbation resulting from the E → Q substitution can be estimated by a Marcus analysis of the electron transfer kinetics in the Ni_a-I¹ → Ni_a-S conversion (Supplemental Discussion). We estimate that the rate of Ni_a-I¹ → Ni_a-S conversion must be retarded by ~10 to become unobservable in the current experiments. To satisfy this, a change in ΔG⁰ of 12 kJ/mol (–120 mV) would be required. This perturbation is quite large for a single conservative point mutation, and we thus favor the interpretation that the E → Q exchange prevents PT rather than ET.

It is interesting to compare the PCET mechanism proposed herein (E–C mechanism in Scheme 1), and the alternatively postulated mechanism for PT via the bridgehead arginine. As noted before, the arginine residue has been shown to aid in H₂ activation in the *E. coli* Hyd-1,⁴⁷ implying it has some role in proton management. It is clear that both arginine and glutamate are necessary for the observed activity of the [NiFe]-H₂ases and both are strictly conserved, but it is unclear how these two observations may be reconciled into a complete and cohesive mechanism for H₂ activation and PT. It is possible for arginine to also be relevant in PT, whereupon binding H₂ in the Ni²⁺ Ni_a-S state, arginine functions as a Lewis base accepting the proton generated by heterolytic H₂ cleavage. Subsequently the hydride, once oxidized, could be transferred out of the active

site via the E–C mechanism described previously. The preference for protonation of arginine relative to cysteine in the Ni_a-S ↔ Ni_a-SR transition could be dictated by the nature of the divalent nickel, which shares less electron density with its sulfur ligands relative to Ni⁺ in Ni_a-I, and thus lowers their pK_a values. This hypothesis would be difficult to reconcile with the putative thiol based proton location in the Ni_a-SR state as proposed by others.^{25,32,89–91} Alternatively, arginine may have an electrostatic role in stabilizing the hydride by its positive charge at the bridgehead position.

CONCLUSIONS

On the basis of steady state and photochemical properties of the WT and E₁₇Q SHI of *Pf* we establish that E₁₇ acts as a proton donor to the active site during the Ni_a-S to Ni_a-C transition and modulates the concerted PCET reaction through proton transfer across a hydrogen bond between a terminally bound cysteine of the active site nickel and E₁₇. While the transient data support E₁₇'s role in PT, the residual enzymatic activity suggests alternative routes are necessary, possibly involving a conserved arginine. This mechanism for controlling PCET chemistry by outer coordination sphere effects could find utility in biomimetic catalyst design and in extending the synthetic modalities for promoting efficient PCET.

ASSOCIATED CONTENT

Supporting Information

The Supporting Information is available free of charge on the ACS Publications website at DOI: 10.1021/jacs.6b07789.

A detailed as presently understood chemical mechanism of [NiFe] H₂ases, H⁺ reduction and H₂ oxidation activity measurements, FTIR spectra of WT and E₁₇Q *Pf* SHI including ν_{CN} region, second derivative FTIR spectra of WT and E₁₇Q *Pf* SHI, peak position summary and comparison of WT and E₁₇Q *Pf* SHI, pH dependent FTIR and TRIR spectra as well as peak position summaries, TRIR spectra of WT and E₁₇Q *Pf* SHI between 5 and 10 μs, single wavelength transients for Ni_a-S and Arrhenius plots for E₁₇Q *Pf* SHI (PDF)

AUTHOR INFORMATION

Corresponding Author

*E-mail: briandyer@emory.edu.

Notes

The authors declare no competing financial interest.

ACKNOWLEDGMENTS

This research was supported by a grant (DE-FG05-95ER20175 to M.W.A.) from the Division of Chemical Sciences, Geosciences and Biosciences, Office of Basic Energy Sciences of the U.S. Department of Energy and by grant (DMR1409851 to R.B.D.) from the National Science Foundation.

REFERENCES

- (1) Vignais, P. M.; Colbeau, A. *Curr. Issues Mol. Biol.* **2004**, *6*, 159–188.
- (2) Vignais, P. M.; Billoud, B. *Chem. Rev.* **2007**, *107*, 4206–4272.
- (3) Peters, J. W.; Schut, G. J.; Boyd, E. S.; Mulder, D. W.; Shepard, E. M.; Broderick, J. B.; King, P. W.; Adams, M. W. W. *Biochim. Biophys. Acta, Mol. Cell Res.* **2015**, *1853*, 1350–1369.

- (4) Greening, C.; Biswas, A.; Carere, C. R.; Jackson, C. J.; Taylor, M. C.; Stott, M. B.; Cook, G. M.; Morales, S. E. *ISME J.* **2016**, *10*, 761–77.
- (5) Fontecilla-Camps, J. C.; Volbeda, A.; Cavazza, C.; Nicolet, Y. *Chem. Rev.* **2007**, *107*, 4273–4303.
- (6) Plumere, N.; Rudiger, O.; Oughli, A. A.; Williams, R.; Vivekananthan, J.; Poller, S.; Schuhmann, W.; Lubitz, W. *Nat. Chem.* **2014**, *6*, 822–827.
- (7) Pershad, H. R.; Duff, J. L. C.; Heering, H. A.; Duin, E. C.; Albracht, S. P. J.; Armstrong, F. A. *Biochemistry* **1999**, *38*, 8992–8999.
- (8) Jones, A. K.; Sillery, E.; Albracht, S. P. J.; Armstrong, F. A. *Chem. Commun.* **2002**, 866–867.
- (9) Madden, C.; Vaughn, M. D.; Diez-Peres, i.; Brown, K. A.; King, P. W.; Gust, D.; Moore, A. L.; Moore, T. A. *J. Am. Chem. Soc.* **2012**, *134*, 1577.
- (10) Rodriguez-Macia, P.; Dutta, A.; Lubitz, W.; Shaw, W. J.; Rudiger, O. *Angew. Chem., Int. Ed.* **2015**, *54*, 12303–7.
- (11) Helm, M. L.; Stewart, M. P.; Bullock, R. M.; DuBois, M. R.; DuBois, D. L. *Science* **2011**, *333*, 863–866.
- (12) Ginovska-Pangovska, B.; Dutta, A.; Reback, M. L.; Linehan, J. C.; Shaw, W. J. *Acc. Chem. Res.* **2014**, *47*, 2621–2630.
- (13) Brazzolotto, D.; Gennari, M.; Queyriaux, N.; Simmons, T. R.; Pécaut, J.; Demeshko, S.; Meyer, F.; Orio, M.; Artero, V.; Duboc, C. *Nat. Chem.* **2016**, advance online publication, DOI 10.1038/nchem.2575.
- (14) Lubitz, W.; Reijerse, E. J.; Messinger, J. *Energy Environ. Sci.* **2008**, *1*, 15–31.
- (15) Elgrishi, N.; McCarthy, B. D.; Rountree, E. S.; Dempsey, J. L. *ACS Catal.* **2016**, *6*, 3644–3659.
- (16) Frey, M.; Fontecilla-Camps, J. C. In *Handbook of Metalloproteins*; Messerschmidt, A., Huber, R., Poulos, T., Weighardt, K., Eds.; John Wiley & Sons: Chichester, U.K., 2001; Vol. 2.
- (17) Greene, B. L.; Wu, C. H.; McTernan, P. M.; Adams, M. W.; Dyer, R. B. *J. Am. Chem. Soc.* **2015**, *137*, 4558–66.
- (18) Volbeda, A.; Charon, M.-H.; Piras, C.; Hatchikian, E. C.; Frey, M.; Fontecilla-Camps, J. C. *Nature* **1995**, *373*, 580–587.
- (19) Montet, Y.; Amara, P.; Volbeda, A.; Vernet, X.; Hatchikian, E. C.; Field, M. J.; Frey, M.; Fontecilla-Camps, J. C. *Nat. Struct. Biol.* **1997**, *4*, 523–526.
- (20) Ogata, H.; Mizoguchi, Y.; Mizuno, N.; Miki, K.; Adachi, S.-i.; Yasuoka, N.; Yagi, T.; Yamauchi, O.; Hirota, S.; Higuchi, Y. *J. Am. Chem. Soc.* **2002**, *124*, 11628–11635.
- (21) Abou Hamdan, A.; Dementin, S.; Liebgott, P. P.; Gutierrez-Sanz, O.; Richaud, P.; De Lacey, A. L.; Rousset, M.; Bertrand, P.; Cournac, L.; Leger, C. *J. Am. Chem. Soc.* **2012**, *134*, 8368–8371.
- (22) Vincent, K. A.; Parkin, A.; Armstrong, F. A. *Chem. Rev.* **2007**, *107*, 4366–4413.
- (23) Hexter, S. V.; Grey, F.; Happe, T.; Climent, V.; Armstrong, F. A. *Proc. Natl. Acad. Sci. U. S. A.* **2012**, *109*, 11516–11521.
- (24) Dementin, S.; Burlat, B.; Fourmond, V.; Leroux, F.; Liebgott, P. P.; Abou Hamdan, A.; Leger, C.; Rousset, M.; Guigliarelli, B.; Bertrand, P. *J. Am. Chem. Soc.* **2011**, *133*, 10211–10221.
- (25) Siegbahn, P. E. M. *Adv. Inorg. Chem.* **2004**, *56*, 101–125.
- (26) Teixeira, V. H.; Soares, C. M.; Baptista, A. M. *Proteins: Struct., Funct., Genet.* **2008**, *70*, 1010–1022.
- (27) Sumner, I.; Voth, G. A. *J. Phys. Chem. B* **2012**, *116*, 2917–2926.
- (28) Ogata, H.; Nishikawa, K.; Lubitz, W. *Nature* **2015**, *520*, 571–4.
- (29) Siebert, E.; Horch, M.; Rippers, Y.; Fritsch, J.; Frielingsdorf, S.; Lenz, O.; Velazquez Escobar, F.; Siebert, F.; Paasche, L.; Kuhlmann, U.; Lendzian, F.; Mroginski, M.-A.; Zebger, I.; Hildebrandt, P. *Angew. Chem., Int. Ed.* **2013**, *52*, 5162–5165.
- (30) Pardo, A.; De Lacey, A. L.; Fernandez, V. M.; Fan, H.-J.; Fan, Y.; Hall, M. B. *JBIC, J. Biol. Inorg. Chem.* **2006**, *11*, 286–306.
- (31) Lill, S. O.; Siegbahn, P. E. M. *Biochemistry* **2009**, *48*, 1056–1066.
- (32) Siegbahn, P. E. M.; Tye, J. W.; Hall, M. B. *Chem. Rev.* **2007**, *107*, 4414–4435.
- (33) Kramer, T.; Kampa, M.; Lubitz, W.; van Gestel, M.; Neese, F. *ChemBioChem* **2013**, *14*, 1898–1905.
- (34) Clegg, W.; Henderson, R. A. *Inorg. Chem.* **2002**, *41*, 1128–1135.
- (35) Henderson, R. A. *J. Chem. Res.* **2002**, 2002, 407–411.
- (36) Weber, K.; Kraemer, T.; Shafaat, H. S.; Weyhermueller, T.; Bill, E.; van Gestel, M.; Neese, F.; Lubitz, W. *J. Am. Chem. Soc.* **2012**, *134*, 20745–20755.
- (37) Gutierrez-Sanchez, C.; Ruediger, O.; Fernandez, V. M.; De Lacey, A. L.; Marques, M.; Pereira, I. A. C. *JBIC, J. Biol. Inorg. Chem.* **2010**, *15*, 1285–1292.
- (38) Marques, M. C.; Coelho, R.; De Lacey, A. L.; Pereira, I. A. C.; Matias, P. M. *J. Mol. Biol.* **2010**, *396*, 893–907.
- (39) Baltazar, C. S. A.; Teixeira, V. H.; Soares, C. M. *JBIC, J. Biol. Inorg. Chem.* **2012**, *17*, 543–555.
- (40) Marques, M. C.; Coelho, R.; Pereira, I. A. C.; Matias, P. M. *Int. J. Hydrogen Energy* **2013**, *38*, 8664–8682.
- (41) Volbeda, A.; Garcin, E.; Piras, C.; de Lacey, A. L.; Fernandez, V. M.; Hatchikian, E. C.; Frey, M.; Fontecilla-Camps, J. C. *J. Am. Chem. Soc.* **1996**, *118*, 12989–12996.
- (42) Higuchi, Y.; Yagi, T.; Yasuoka, N. *Structure* **1997**, *5*, 1671–1680.
- (43) Matias, P. M.; Soares, C. M.; Saraiva, L. M.; Coelho, R.; Morais, J.; Le Gall, J.; Carrondo, M. A. *JBIC, J. Biol. Inorg. Chem.* **2001**, *6*, 63–81.
- (44) De Lacey, A. L.; Fernandez, V. M.; Rousset, M.; Cavazza, C.; Hatchikian, E. C. *JBIC, J. Biol. Inorg. Chem.* **2003**, *8*, 129–134.
- (45) Dementin, S.; Burlat, B.; De Lacey, A. L.; Pardo, A.; Adryanczyk-Perrier, G.; Guigliarelli, B.; Fernandez, V. M.; Rousset, M. *J. Biol. Chem.* **2004**, *279*, 10508–10513.
- (46) Galvan, I. F.; Volbeda, A.; Fontecilla-Camps, J. C.; Field, M. J. *Proteins: Struct., Funct., Genet.* **2008**, *73*, 195–203.
- (47) Evans, R. M.; Brooke, E. J.; Wehlin, S. A.; Nomerotskaia, E.; Sargent, F.; Carr, S. B.; Phillips, S. E.; Armstrong, F. A. *Nat. Chem. Biol.* **2015**, *12*, 46–50.
- (48) Szori-Doroghazi, E.; Maroti, G.; Szori, M.; Nyilasi, A.; Rakhely, G.; Kovacs, K. L. *PLoS One* **2012**, *7*, e34666.
- (49) Peters, J. W.; Lanzilotta, W. N.; Lemon, B. J.; Seefeldt, L. C. *Science* **1998**, *282*, 1853–1858.
- (50) Esselborn, J.; Lambertz, C.; Adamska-Venkatesh, A.; Simmons, T.; Berggren, G.; Noth, J.; Siebel, J.; Hemschemeier, A.; Artero, V.; Reijerse, E.; Fontecave, M.; Lubitz, W.; Happe, T. *Nat. Chem. Biol.* **2013**, *9*, 607–609.
- (51) Mulder, D. W.; Ratzloff, M. W.; Bruschi, M.; Greco, C.; Koonce, E.; Peters, J. W.; King, P. W. *J. Am. Chem. Soc.* **2014**, *136*, 15394–15402.
- (52) Camara, J. M.; Rauchfuss, T. B. *Nat. Chem.* **2011**, *4*, 26–30.
- (53) Harms, M. J.; Schlessman, J. L.; Sue, G. R.; Garcia-Moreno, E. B. *Proc. Natl. Acad. Sci. U. S. A.* **2011**, *108*, 18954–18959.
- (54) Guillen Schlippe, Y. V.; Hedstrom, L. *Arch. Biochem. Biophys.* **2005**, *433*, 266–278.
- (55) Greene, B. L.; Wu, C.-H.; Vansuch, G. E.; Adams, M. W. W.; Dyer, R. B. *Biochemistry* **2016**, *55*, 1813–1825.
- (56) Chandrayan, S. K.; Wu, C.-H.; McTernan, P. M.; Adams, M. W. W. *Protein Expression Purif.* **2015**, *107*, 90–94.
- (57) Bertrand, P.; Dole, F.; Asso, M.; Guigliarelli, B. *JBIC, J. Biol. Inorg. Chem.* **2000**, *5*, 682–691.
- (58) Wang, H.; Ralston, C. Y.; Patil, D. S.; Jones, R. M.; Gu, W.; Verhagen, M.; Adams, M.; Ge, P.; Riordan, C.; Marganian, C. A.; Mascharak, P.; Kovacs, J.; Miller, C. G.; Collins, T. J.; Brooker, S.; Croucher, P. D.; Wang, K.; Steifel, E. I.; Cramer, S. P. *J. Am. Chem. Soc.* **2000**, *122*, 10544–10552.
- (59) George, S. J.; Kurkin, S.; Thorneley, R. N. F.; Albracht, S. P. J. *Biochemistry* **2004**, *43*, 6808–6819.
- (60) Kwan, P.; McIntosh, C. L.; Jennings, D. P.; Hopkins, R. C.; Chandrayan, S. K.; Wu, C. H.; Adams, M. W.; Jones, A. K. *J. Am. Chem. Soc.* **2015**, *137*, 13556–65.
- (61) de Lacey, A. L.; Hatchikian, E. C.; Volbeda, A.; Frey, M.; Fontecilla-Camps, J. C.; Fernandez, V. M. *J. Am. Chem. Soc.* **1997**, *119*, 7181–7189.
- (62) Cammack, R.; Patil, D. S.; Hatchikian, C. E.; Fernandez, V. M. *Biochim. Biophys. Acta, Protein Struct. Mol. Enzymol.* **1987**, *912*, 98–109.

- (63) De Lacey, A. L.; Fernandez, V. M. *Chem. Rev.* **2007**, *107*, 4304–4330.
- (64) Prince, R. C.; Adams, M. W. W. *J. Biol. Chem.* **1987**, *262*, 5125–8.
- (65) Van der Zwaan, J. W.; Albracht, S. P. J.; Fontijn, R. D.; Slater, E. C. *FEBS Lett.* **1985**, *179*, 271–7.
- (66) Kellers, P.; Pandelia, M.-E.; Currell, L. J.; Goerner, H.; Lubitz, W. *Phys. Chem. Chem. Phys.* **2009**, *11*, 8680–8683.
- (67) Tai, H.; Nishikawa, K.; Suzuki, M.; Higuchi, Y.; Hirota, S. *Angew. Chem., Int. Ed.* **2014**, *53*, 13817–13820.
- (68) Greene, B. L.; Joseph, C. A.; Maroney, M. J.; Dyer, R. B. *J. Am. Chem. Soc.* **2012**, *134*, 11108–11111.
- (69) Murphy, B. J.; Hidalgo, R.; Roessler, M. M.; Evans, R. M.; Ash, P. A.; Myers, W. K.; Vincent, K. A.; Armstrong, F. A. *J. Am. Chem. Soc.* **2015**, *137*, 8484–9.
- (70) Hidalgo, R.; Ash, P. A.; Healy, A. J.; Vincent, K. A. *Angew. Chem., Int. Ed.* **2015**, *54*, 7110–3.
- (71) Murphy, B. J.; Hidalgo, R.; Roessler, M. M.; Evans, R. M.; Ash, P. A.; Myers, W. K.; Vincent, K. A.; Armstrong, F. A. *J. Am. Chem. Soc.* **2015**, *137*, 8484–8489.
- (72) Roessler, M. M.; Evans, R. M.; Davies, R. A.; Harmer, J.; Armstrong, F. A. *J. Am. Chem. Soc.* **2012**, *134*, 15581–15594.
- (73) Pandelia, M.-E.; Infossi, P.; Stein, M.; Giudici-Orticoni, M.-T.; Lubitz, W. *Chem. Commun.* **2012**, *48*, 823–5.
- (74) Foerster, S.; Stein, M.; Brecht, M.; Ogata, H.; Higuchi, Y.; Lubitz, W. *J. Am. Chem. Soc.* **2003**, *125*, 83–93.
- (75) Chang, C. J.; Chang, M. C. Y.; Damrauer, N. H.; Nocera, D. G. *Biochim. Biophys. Acta, Bioenerg.* **2004**, *1655*, 13–28.
- (76) Huynh, M. H. V.; Meyer, T. J. *Chem. Rev.* **2007**, *107*, 5004–5064.
- (77) Hammes-Schiffer, S. *J. Am. Chem. Soc.* **2015**, *137*, 8860–8871.
- (78) Bryant, F. O.; Adams, M. W. *J. Biol. Chem.* **1989**, *264*, 5070–9.
- (79) Arendsen, A. F.; Veenhuizen, P. T. M.; Hagen, W. R. *FEBS Lett.* **1995**, *368*, 117–21.
- (80) Tard, C.; Pickett, C. J. *Chem. Rev.* **2009**, *109*, 2245–2274.
- (81) Perotto, C. U.; Marshall, G.; Jones, G. J.; Stephen Davies, E.; Lewis, W.; McMaster, J.; Schroder, M. *Chem. Commun.* **2015**, *51*, 16988–91.
- (82) Chambers, G. M.; Huynh, M. T.; Li, Y.; Hammes-Schiffer, S.; Rauchfuss, T. B.; Chambers, G. M.; Rauchfuss, T. B.; Reijerse, E.; Lubitz, W. *Inorg. Chem.* **2016**, *55*, 419–431.
- (83) Schilter, D.; Camara, J. M.; Huynh, M. T.; Hammes-Schiffer, S.; Rauchfuss, T. B. *Chem. Rev.* **2016**, *116*, 8693–8749.
- (84) Eberhardt, N. A.; Guan, H. *Chem. Rev.* **2016**, *116*, 8373–8426.
- (85) Ogo, S.; Ichikawa, K.; Kishima, T.; Matsumoto, T.; Nakai, H.; Kusaka, K.; Ohhara, T. *Science* **2013**, *339*, 682–684.
- (86) Ogo, S. *Coord. Chem. Rev.* **2016**, Ahead of Print, DOI [10.1016/j.ccr.2016.07.001](https://doi.org/10.1016/j.ccr.2016.07.001).
- (87) Alben, J. O.; Moh, P. P.; Fiamingo, F. G.; Altschuld, R. A. *Proc. Natl. Acad. Sci. U. S. A.* **1981**, *78*, 234–237.
- (88) Abou-Hamdan, A.; Ceccaldi, P.; Lebrette, H.; Gutierrez-Sanz, O.; Richaud, P.; Cournac, L.; Guigliarelli, B.; De Lacey, A. L.; Leger, C.; Volbeda, A.; Burlat, B.; Dementin, S. *J. Biol. Chem.* **2015**, *290*, 8550–8558.
- (89) Stein, M.; Lubitz, W. *Phys. Chem. Chem. Phys.* **2001**, *3*, 5115–5120.
- (90) Bruschi, M.; Tiberti, M.; Guerra, A.; De Gioia, L. *J. Am. Chem. Soc.* **2014**, *136*, 1803–1814.
- (91) Dong, G.; Ryde, U. *JBIC, J. Biol. Inorg. Chem.* **2016**, *21*, 383–94.